Spatial stress correlations in strong colloidal gel systems

Divas Singh Dagur,[1] Chandana Mondal,[2] and Saikat Roy[1,*]
[1]*Department of Chemical Engineering, Indian Institute of Technology Ropar, Rupnagar, Punjab 140001, India*
[2]*UGC-DAE Consortium for Scientific Research, University Campus, Khandwa Road, Indore 452017, India*

(Received 14 May 2022; revised 26 May 2023; accepted 12 July 2023; published 26 July 2023)

Colloidal gel systems exhibit increasingly slow relaxation and ultra-long-ranged spatial correlations of the dynamics similar to other jammed materials. These cooperative dynamics point to the presence of long-ranged stress correlation in these systems, which remain largely uninvestigated in the literature. In this work, we systematically investigate the nature of stress correlations in soft colloidal gel materials in the limit of moderate to high packing fractions and strong attraction. In this regime, centrosymmetric potential description for particle interaction fails as strong attraction can lead to frictional contacts, as shown explicitly in previous experiments. Accordingly, we model the system similarly to the cohesive granular media with Langevin dynamics to incorporate the effects of rolling and sliding resistant contacts and thermal fluctuations. We show that the spatial stress correlations are long ranged with very slow spatial decay close to the gel point. Similarly to previous studies on the frictional granular matter, the full stress autocorrelation matrix is dictated by the pressure and torque autocorrelations due to mechanical balance and material isotropy constraints. Surprisingly, it is observed that the gel materials do not behave as a normal elastic solid *close to the gel point* as assumed loosely in the literature because the real-space pressure fluctuations decay slower than normal. Furthermore, we link the abnormal pressure fluctuations to the non-hyperuniform behavior of the system (granular matter and gel) with respect to the local packing fraction fluctuations, thus relating the deviations from the normal elastic behavior across various jammed systems under a common framework.

DOI: 10.1103/PhysRevB.108.024106

I. INTRODUCTION

Colloids form disordered solids in seemingly different ways based on the interparticle potential and the volume fraction. At a high volume fraction, crowded interaction between hard-sphere colloids gives rise to the caging effect and dynamical arrest, which results in the repulsive colloidal glass [1]. Increasing the strength of attraction leads to the formation of attractive glass. In contrast, colloids form space-filling percolated networks of fractal clusters and manifest solid-like properties at very low volume fractions under strong attraction. Previous studies primarily focused on the low volume fractions regime [2] for better imaging of the structural evolution. In contrast, the behavior of the colloidal gel systems in the intermediate volume fractions regime is more complex and less evident since the system will be affected by both the caging effects and the fractal correlations. One of the critical unexplored issues in the colloidal gel community is understanding the mechanical response of the colloidal gel in the limit when the gels are neither too dilute nor too dense, and the structural arrest is driven by the complex interplay between the steric hindrance and attractive bonding. It is even more challenging to relate the behavior of such a colloidal gel system to that of other amorphous solids formed at relatively high packing fractions, such as glass and granular materials, under a unified framework.

Unlike perfect crystals, amorphous solids have many microscopic degrees of freedom in their equilibrium states as it is not necessarily the global minimum of the potential energy surface; instead, it is at some local minimum. These metastable states are known as inherent states, and the characterization of these states is difficult as the system properties are strongly dependent on the preparation protocol. Although properties of the inherent states vary across different amorphous media, rare universality in some of the macroscopic properties, such as vibrational properties, is found. Simulations on model glass [3], granular matter [3,4], and supercooled liquids [5–7] show a power-law decay of spatial shear stress correlation ($1/r^d$ in d dimension) with quadrupolar anisotropy. Experiments on colloidal gel systems using time-resolved light scattering and photon correlation imaging suggest the presence of ultra-long-ranged spatial correlation [2,8] of dynamics which span up to the system size far greater than any relevant length scale used to describe the mechanical response of the fractal colloidal gel. Interestingly, the bond-breaking event in the gel network has nonlocal consequences [9,10] and corresponding large rearrangements far away from the rupture event. Very little understanding is available in the literature regarding the physical mechanism behind these long-ranged cooperative dynamics in the colloidal gel system and its connection to the broad class of amorphous solids showing similar behavior. In this article, we show the presence of long-ranged stress correlations in the colloidal gel network, which is the plausible reason for the long-ranged dynamical correlations.

On the theoretical front, Lemaître showed that mechanical balance and material isotropy are sufficient to capture these long-range stress correlations without the involvement of any

*Corresponding author: saikat.roy@iitrpr.ac.in

elasticity [11–13]. Although simulation data on the granular matter and model glass support the theoretical predictions, no study has been devoted to understanding the nature of stress correlations and applicability of the existing theories in strongly attractive systems such as colloidal gels in the dense limit. When the thermal fluctuations are negligible compared to the strong attractive potential, $-U/k_BT \geqslant 20$, dense colloidal suspension rapidly forms thermally irreversible microstructure that can support an external load. The mechanism of macroscopic aging and thixotropy observed in such systems is nontrivial and cannot be attributed to structural aging since the microstructure gets completely frozen in the limit of a strong attraction and high packing fraction. Recent experiments [14,15] studied similar systems and demonstrated a correlation between the contact scale aging and the macroscopic shear modulus and yield stress aging. Another plausible way the system can age is by redistributing the quenched stress heterogeneities created during the structural arrest via small long-range-correlated displacements of its constituents. Such strongly aggregating dense colloidal gel systems find applications in diverse areas like foods, pharmaceuticals, cosmetics, aerogels, and drug delivery. Hence, it will be of great interest to find out whether these systems present long-range correlations or not since the nature of the correlation will regulate the macroscopic mechanical response and aging features of the colloidal gel. It is also essential to test whether the existing theories [11,12] can capture the stress correlations in this type of soft gel material formed at relatively low packing fractions with large structural and mechanical heterogeneity compared to other amorphous systems.

In this work, we show via numerical simulations that the stress correlations in the colloidal gel are entirely determined by two spatially isotropic functions: the pressure and torque autocorrelations. We find that pressure autocorrelations show divergence at small wave numbers close to the gel point and far away from it; the slope of the divergence decreases. It implies that the elastic theory, generally applied to the gel network at low pressure, must be revisited. Although the gel network is formed at low packing fractions compared to granular materials, the symmetry and nature of the stress autocorrelation matrix show remarkable universal features.

II. SIMULATION METHODOLOGY AND THEORETICAL BACKGROUND

Simulation of isotropic compression of flocculated colloidal particulate networks is performed using open source code, the Large-scale Atomic/Molecular Massively Parallel Simulator (LAMMPS) [16]. Under compression, the spatial and temporal evolution of the colloidal gel network will mainly depend on the hydrodynamic and elastic interactions. Our study employs very slow strain rates ($\approx 10^{-5}\ \mathrm{s}^{-1}$) to mimic quasistatic compression, and as a result of that, the ratio of the drag force ($\eta\dot{\epsilon}$) to elastic force ($G\epsilon$) becomes negligible. Here, η, $\dot{\epsilon}$, G, and ϵ represent solvent viscosity, strain rate, particle modulus, and strain, respectively. Previous experimental studies [17,18] also show that the hydrodynamic interactions do not play a dominant role in the dynamics when the strain rates are small and a system-spanning network has been formed. Incorporating the hydrodynamics will only lead to a lower packing fraction for the structural arrest and different fractal dimension [19], which is expected to have a negligible influence on the nature of stress correlations. In light of these experiments and the order-of-magnitude calculation of the relevant forces, we exclude the hydrodynamic forces in the simulation. Most of the previous simulations [20] on the gel system consider central forces, sometimes with an angle-dependent three-body term, to impart angular rigidity to the interparticle bonds. But in the limit of moderate to high packing fraction, due to the surface asperities and strong attraction, the colloidal particles may come into contact, and consequently, tangential interactions like sliding and rolling effects will become important, as observed in the experiments and simulations [14,15,21–24]. Such effects can easily be incorporated by modeling the colloidal gel system as cohesive granular media under stochastic forcing, and recent simulations [25–29] show encouraging results in capturing the rheology of the colloidal gel system with the same model. In this work, we also model the colloidal gel system with the help of the DEM (discrete-element method) simulation [30] generally applied for the granular materials. Only adding adhesion to the dry granular materials will not resemble the colloidal gel system; additionally, one needs stochastic forcing to obtain a fractal gel-like structure. So, our simulation is completely different from the simulation generally employed for wet granular materials under no thermal fluctuations.

The simulation starts with the random placement of $N = 16\,000$ soft elastic disks of diameter D in a two-dimensional periodic square box of size $295D$, corresponding to a packing fraction, $\phi \approx 0.1$. The contact deformation is modeled as Hookean, and the normal part of the elastic repulsive force is given as $F_N^{e,ij} = -k_n \delta n_{ij}$ where k_n is the normal stiffness. This force acts when the overlap distance between two particles $\delta n_{ij} < 0$. In addition to the elastic part, normal viscous damping, $-\gamma_n \underline{v}_{n_{ij}}$ (here $\underline{v}_{n_{ij}}$ is the normal component of the relative velocity between particle pair i and j and γ_n is the normal viscoelastic damping coefficient) is also added to obtain the static equilibrium in a reasonable time. Similarly, for the tangential part, the force F_T^{ij} varies linearly with the tangential overlap until the initiation of sliding, which takes place when $F_T^{ij} \geqslant \pm\mu F_N^{e,ij}$, where μ is the sliding friction coefficient. We also add tangential damping similar to normal damping. A constant attractive force of magnitude F_0 acting center to center between two particles is introduced when a contact is made. It should be noted that the Coulomb inequality applies to the repulsive elastic normal force only. The rolling resistance between the particles is incorporated [21] and modeled similarly to the contact elasticity and friction for the sliding mode. The rolling force [31] is given as

$$\underline{F}_r^{ij} = k_r \underline{\delta}_{\mathrm{roll}} - \gamma_r \underline{v}_{\mathrm{roll}}, \tag{1}$$

where k_r is the rolling stiffness, $\underline{\delta}_{\mathrm{roll}}$ is the rolling displacement, γ_r is the damping constant for the rolling mode, and $\underline{v}_{\mathrm{roll}}$ is the relative rolling velocity. Like sliding friction, the rolling force is limited by $\mu_r F_N^{e,ij}$, where μ_r denotes the rolling friction coefficient. In this work, $k_n = k_t = 2 \times 10^5$ N/m, $k_r = k_t/10$, $\mu = \mu_r = 0.5$, $\gamma_n = \gamma_t = \gamma_r = 50$ kg/s, and $F_0/k_nD = 0.0025$. The pressure values reported in the main text are in SI units. The particles are given random kicks to

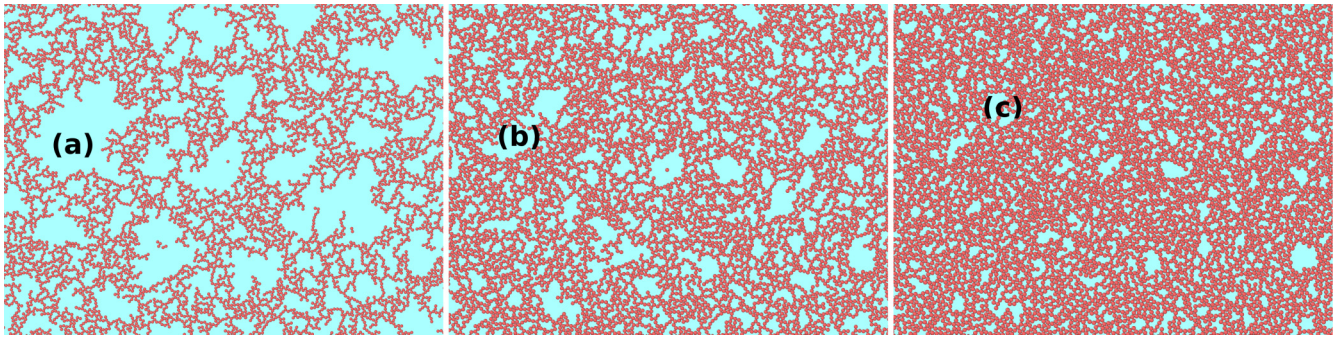

FIG. 1. Evolution of the gel microstructure under compression. (a) Initial low packing fraction, $\phi = 0.22$, showing the presence of large voids and density heterogeneities. (b) Intermediate packing fraction, $\phi = 0.3$, with small voids after structural rearrangement under compression. (c) Final compact state, $\phi = 0.44$, with minimal density heterogeneity.

their translational and rotational degrees of freedom, compensated by a damping term. The Langevin equation is solved to update the particle positions and velocities,

$$m_i \frac{d^2\underline{x}_i}{dt^2} = \underline{F}_i - m_i\gamma_t \frac{d\underline{x}_i}{dt} + \underline{f}_i(t), \tag{2}$$

$$I_i \frac{d^2\underline{\theta}_i}{dt^2} = \underline{T}_i - I_i\gamma_r \frac{d\underline{\theta}_i}{dt} + \underline{L}_i(t), \tag{3}$$

where $\underline{f}_i(t)$ and $\underline{L}_i(t)$ are respectively a δ-correlated random force/torque having zero mean with the following properties:

$$\langle \underline{f}_i(t) \cdot \underline{f}_j(t+\tau)\rangle = 2\Gamma\delta(\tau)\delta_{ij};$$
$$\langle \underline{L}_i(t) \cdot \underline{L}_j(t+\tau)\rangle = 2\Gamma\delta(\tau)\delta_{ij}. \tag{4}$$

Here γ_t and γ_r are translational and rotational damping coefficients, m_i and I_i, are the mass and moment of inertia of the particle i, $\underline{F}_i$ and $\underline{T}_i$ are the force and torque due to interparticle interactions, Γ is the strength of fluctuations, and $\underline{x}_i$ and $\underline{\theta}_i$ denote the translational and rotational degrees of freedom.

Thermal fluctuations will lead to the flocculation of particles as the interaction is attractive, and the flocs are brought closer by the isotropic compression. We employ compression on top of the thermal fluctuations for the rapid formation of the percolating network. In fact, as per our simulation protocol, the gel formation process involves two timescales: one is the compression timescale and another is the Brownian timescale. Fast compression will lead to higher gelation concentration and dense microstructure, whereas slow compression will give rise to open microstructure and lower gel point. One can tune the timescale of the compression to obtain different microstructures at a given temperature. Once the flocs connect to form a system spanning percolating network at the gel point, Brownian motion has little effect on the dynamics since the attractive potential is much stronger than the thermal force (strong gel). The dynamics of the strong gel are determined by the internal stress field induced during the structural arrest at the gel point and the imposed deformation field. When the thermal fluctuations are comparable to the attraction, weak gels are formed, and the Brownian forces will have a significant role in the microscopic dynamics of the gel network. We focus only on the strong gels in this study; hence the rearrangement of the microstructure due to thermal motion is not possible.

We compress the gel network isotropically and quasistatically at a very slow strain rate to various target pressures. The strain rates are chosen in such a way [32] that the product of the natural inertial timescale ($\sqrt{mD/F_0}$) associated with the characteristic attraction force and the maximum strain rate is very small ($\sim 10^{-6}$). In this slow compression limit, the inertial effects are significantly reduced. The system is then allowed to reach mechanical equilibrium (i.e., total force and torque on each particle are negligibly small [$O(10^{-7})$] with almost zero kinetic energy [$O(10^{-16})$]) at different target pressures before we start measuring the stress correlations. The packing fraction ϕ, corresponding to $P = 2.75$ N/m, is 0.22, and we went up to $\phi = 0.44$ corresponding to the highest pressure investigated, $P = 328$ N/m. In Fig. 1, we present the snapshots of the configurations at different packing fractions showing the structural evolution of the colloidal gel system under compression. The first stable percolating network forms at around $\phi \approx 0.21$ with large density inhomogeneities, and as the compression proceeds, voids collapse, and the structure becomes compact with lesser density fluctuations. For each pressure, we performed simulations with ten different independent initial configurations and found minimal variations (less than 5%) in the properties of interest. We construct the stress field from the particle-level force data and calculate all the correlations between different stress components. The stress tensor in Fourier space [33] reads

$$\sigma_{\gamma\delta\underline{q}} = \frac{1}{2A}\sum_{i,j,i\neq j} F_{ij}^{\gamma} r_{ij}^{\delta} \frac{e^{-i\underline{q}\cdot\underline{r}_i} - e^{-i\underline{q}\cdot\underline{r}_j}}{i\underline{q}\cdot\underline{r}_{ij}}, \tag{5}$$

where A is the system area, $\underline{q}$ is allowed wave vector, γ, δ denote the Cartesian coordinates, $\underline{F}_{ij}$ is the interparticle force, $\underline{r}_i$ is the position of particle i, and $\underline{r}_{ij}$ is the radial vector between particles i and j. As the stress tensor is nonsymmetric because of noncentral interactions, this representation will have four spherical components in Fourier space [12]:

$$\sigma_{1\underline{q}} = -\tfrac{1}{2}(\sigma_{xx\underline{q}} + \sigma_{yy\underline{q}}),$$
$$\sigma_{2\underline{q}} = \tfrac{1}{2}(\sigma_{xx\underline{q}} - \sigma_{yy\underline{q}}),$$
$$\sigma_{3\underline{q}} = \tfrac{1}{2}(\sigma_{xy\underline{q}} + \sigma_{yx\underline{q}}),$$
$$\sigma_{4\underline{q}} = \tfrac{1}{2}(\sigma_{xy\underline{q}} - \sigma_{yx\underline{q}}).$$

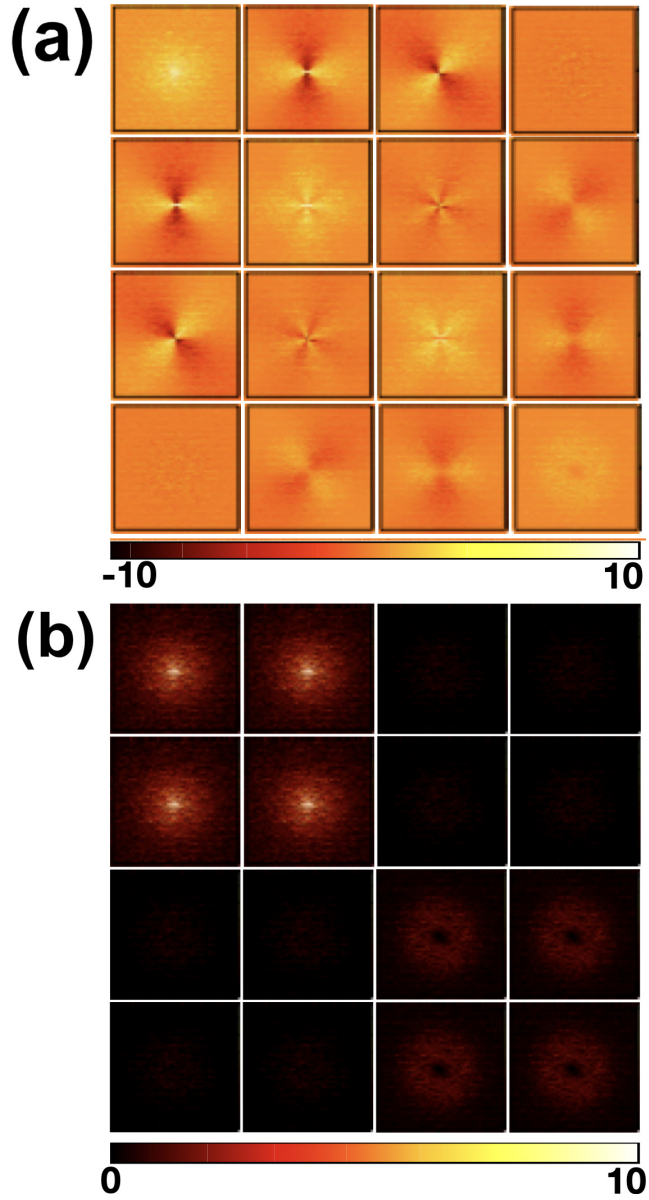

FIG. 2. (a) Fourier space stress correlation fields in the Cartesian frame, S_{abq}, for $P = 2.75$ ($\phi = 0.22$) are shown as a matrix (symmetric). The first row corresponds to 1, 1; 1, 2; 1, 3; and 1, 4 components, and similarly, other components are shown in the subsequent rows. (b) The same field in the radial frame, $\mathbb{S}_{abq}$.

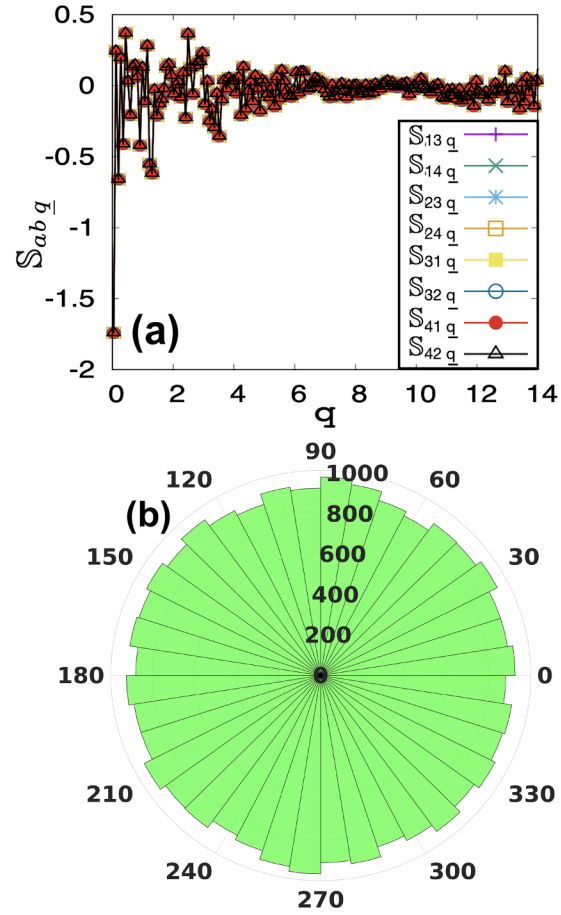

FIG. 3. (a) Angle-averaged off-diagonal correlations $\mathbb{S}_{abq}$, $ab = 13, 14, 23, 24, 31, 32, 41, 42$, for $P = 2.75$ ($\phi = 0.22$). (b) Contact orientation distribution at $P = 2.75$ ($\phi = 0.22$). Same distribution is observed at $P = 328$ ($\phi = 0.44$) (not shown)

III. STRESS CORRELATIONS AND ISOTROPY

If the system is translation invariant, the autocorrelation matrix of these Cartesian spherical stress components in Fourier space reads as $\underset{\approx}{S}_{\underline{q}} = \frac{1}{A}\langle \underset{\sim}{\sigma}_{\underline{q}}\, \underset{\sim}{\sigma}^{*}_{\underline{q}}\rangle_c$, where * denotes the complex conjugate and $\langle\ \rangle_c$ represents the second cumulant for the ensemble average. $\underset{\approx}{S}_{\underline{q}}$ is calculated for all the stress components defined earlier. We show the same in Fig. 2(a) as a matrix of fields for pressure $P = 2.75$, which is very close to the gel point. We observe similar fields for $P = 328$ (not shown). Only pressure $S_{11\,\underline{q}}$ and torque $S_{44\,\underline{q}}$ autocorrelations and their cross correlations are isotropic and the rest are anisotropic. The whole matrix is clearly symmetric with unexpected anisotropic cross correlations between the torque and other fields as previously observed in granular matter [11,12]. Although the gel network is formed at a very low packing fraction with fractal correlations, it is very surprising that the structure of the stress autocorrelation fields bears a striking resemblance to that in frictional granular matter. To understand the role of material isotropy, we now calculate the Fourier space autocorrelations matrix in the radial frame with basis ($\underline{e}_q$, $\underline{e}_\phi$). The corresponding stress vector components are given as

$$\sigma^{\hat{q}}_{1\,\underline{q}} = -\tfrac{1}{2}(\sigma_{qq\,\underline{q}} + \sigma_{\phi\phi\,\underline{q}}),$$

$$\sigma^{\hat{q}}_{2\,\underline{q}} = \tfrac{1}{2}(\sigma_{qq\,\underline{q}} - \sigma_{\phi\phi\,\underline{q}}),$$

$$\sigma^{\hat{q}}_{3\,\underline{q}} = \tfrac{1}{2}(\sigma_{q\phi\,\underline{q}} + \sigma_{\phi q\,\underline{q}}),$$

$$\sigma^{\hat{q}}_{4\,\underline{q}} = \tfrac{1}{2}(\sigma_{q\phi\,\underline{q}} - \sigma_{\phi q\,\underline{q}}),$$

where $\hat{q} \equiv \underline{q}/q$ denotes the direction vector in reciprocal space. The autocorrelation matrix of these radial components is given by $\underset{\approx}{\mathbb{S}}_{\underline{q}} = \frac{1}{A}\langle \underset{\sim}{\sigma}^{\hat{q}}_{\underline{q}} (\underset{\sim}{\sigma}^{\hat{q}}_{\underline{q}})^{*}\rangle_c$. It can be easily shown [12] that under the constraint of material balance and isotropy, the structure of the radial autocorrelation fields contains just two

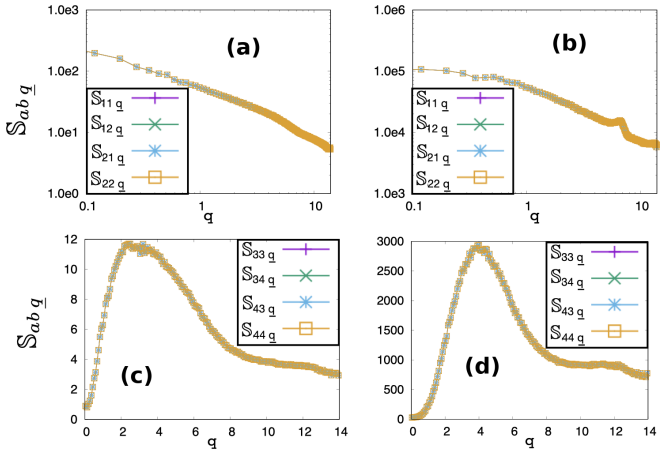

FIG. 4. Plot of the pressure autocorrelation function $\mathbb{S}_{ab\underline{q}}$, $ab = 11, 12, 21, 22$, for (a) $P = 2.75$ ($\phi = 0.22$) and (b) $P = 328$ ($\phi = 0.44$). Plot of the torque density autocorrelation function $\mathbb{S}_{ab\underline{q}}$, $ab = 33, 34, 43, 44$, for (c) $P = 2.75$ ($\phi = 0.22$) and (d) $P = 328$ ($\phi = 0.44$).

spatially isotropic functions, namely pressure and torque autocorrelations. The same field is shown in Fig. 2(b), depicting excellent agreement with the theory, which implies that the constraints of mechanical balance and material isotropy are indeed satisfied in our system. The off-diagonal components, expected to be identically zero from theory, show remnant fluctuations. In previous studies [12], these residual fluctuations were attributed to numerical inaccuracy, which is indeed true in the present study as angle averaging [see Fig. 3(a)] strongly reduces the fluctuations revealing their random nature. We also compute the contact orientation distribution and find that the contact network remains isotropic throughout the deformation [see Fig. 3(b)]. This provides additional proof of the material isotropy.

Next, we investigate the pressure and torque autocorrelations (Fig. 4). The torque correlation approaches zero in the $q \to 0$ limit for high pressure, whereas it reaches a finite nonzero value for low pressure. It implies that the gel network carries some long-range torque correlation close to the gel point, which gives rise to a correlated system spanning vortex-like motions [see Fig. 5(a)], which precludes the applicability of classical elasticity theory. At high pressure, the torque fluctuations become hyperuniform leading to localized nonaffine motions [Fig. 5(b)]. The pressure correlations show divergence: $q^{-\nu}$ in the small-wave-number limit for low pressure, whereas it approaches almost a constant value as $q \to 0$ for high pressure. The divergence exponent is measured by averaging over all the components of relevant correlations (11,12,21,22) [Fig. 4(a)], and it turns out that the pressure autocorrelations show a divergence of the form $q^{-0.51\pm0.02}$ at $P = 2.75$.

IV. PRESSURE FLUCTUATIONS

In earlier works [12], it was shown that the normal elastic behavior demands normal fluctuations of pressure and torque density. The torque autocorrelations are not hyperuniform for the colloidal gel at low pressure. However, at high pressure $P = 328$, torque autocorrelations become hyperuniform, and thus the stress autocorrelation is fully determined by the pressure fluctuations statistics. Hence, we compute the pressure fluctuations in real space by randomly placing a circular window of radius R and measuring the variance of pressure $V_P(R)$ due to circle-to-circle and sample-to-sample fluctuations,

$$V_P(R) \equiv \langle P(R)^2 \rangle - \langle P(R) \rangle^2 \sim \frac{1}{R^\eta}. \tag{6}$$

In the case of normal fluctuations, the variance is expected to decay as the inverse area of the probing window, i.e., $1/R^2$,

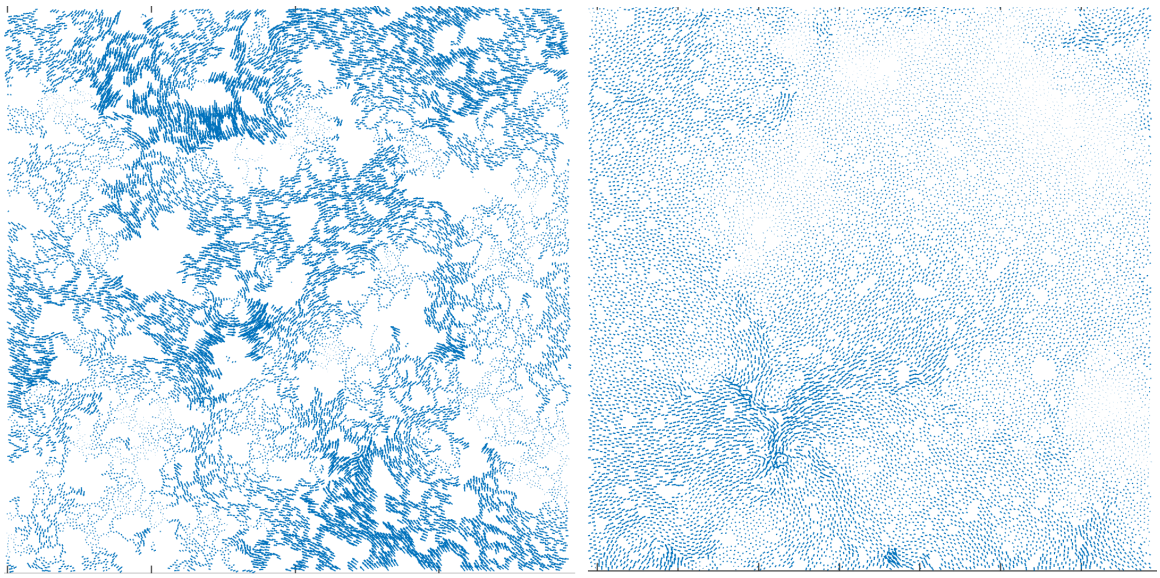

FIG. 5. Nonaffine part of the displacement field, i.e., displacement of a particle (from its reference position) subtracted from the corresponding displacement that would have occurred had the particle moved affinely as per the macroscopic strain. (a) Colloidal gel system at low pressure, $P = 2.75$ ($\phi = 0.22$). (b) Colloidal gel system at high pressure, $P = 328$ ($\phi = 0.44$).

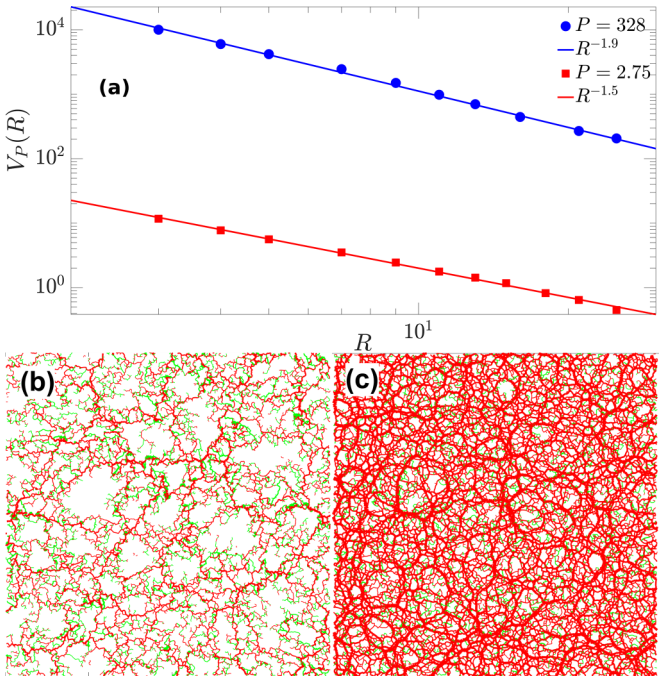

FIG. 6. (a) Pressure variance as a function of the radius of the probing circular window. The solid straight lines are the best linear fits and represent the power law with exponent -1.5 ± 0.02 and -1.9 ± 0.03, respectively, for low and high pressure. (b) Force chains in colloidal gel sample, $P = 2.75$ ($\phi = 0.22$), (c) $P = 328$ ($\phi = 0.44$). The compressive force is drawn in red, whereas the green color represents the tensile force. We compute the magnitude of the pairwise normal force and scale the line (joining two particle centers for a pairwise interaction) thickness as per the magnitude.

and consequently, the stress or pressure correlation shows no divergence in the low-wave-number limit. In a more generic sense, the exponent of the divergence in the Fourier space is related to the exponent of the decay of the pressure fluctuations in real space as $\nu = 2 - \eta$ [12]. In Fig. 6(a) we show the pressure fluctuations as a function of R for both pressures, $P = 2.75$ and $P = 328$. For low pressure, $V_P(R)$ decays like $R^{-1.5}$, which is slower than the normal decay. This slope is in line with the slope of the divergence in the stress correlations in Fourier space. Note that although the torque correlations are not hyperuniform at low pressure, the long-range stress correlations are predominantly decided by the pressure fluctuations. Far above the gel point, the pressure fluctuations become approximately normal with a slope of 1.9, leading to almost divergence-free behavior of the pressure autocorrelations in the small-q limit. Again, the statistics of the pressure fluctuations determine the long-distance decay of the stress correlations.

Force chains. To understand the microscopic origin of the long-distance decay behavior for low and high pressures, we plotted the real-space map of the force chains in Figs. 6(b) and 6(c). One can clearly observe the inhomogeneity in the force chain network at low pressure created due to the presence of large voids in the gel contact network. We also determine the characteristic chain length as a function of the packing fraction above which the particle network looks uniform. The local particle density is calculated in square boxes of increasing length, and it shows little fluctuations when the size of the box is larger than the correlation length, which corresponds to the characteristic chain length [26]. Due to the finite system size, the correlation length at each packing fraction is taken as the box size, where the standard deviation of the local density normalized by the global density becomes 0.5. For a fractal network with an invariant fractal dimension, the correlation length ξ shows power-law decay with the packing fraction with an exponent $-1/(d - d_f)$ (see Fig. 7), where d_f is the fractal dimension and d is the Euclidean dimension. Our data suggest a fractal dimension of 1.44. The gel network is fractal in nature at low pressure, and the inhomogeneity in the force chain network is created due to the strong fractal-like structural correlations, whereas the frictional granular media is not fractal but still gives rise to strong heterogeneity in the force chains [11,12]. As the frictional granular matter jams at high packing fractions, these anomalous correlations, once formed, do not relax through structural rearrangement. In contrast, under compression, the gel network loses fractal correlations and undergoes structural rearrangement through the collapse of voids leading to homogeneous and isotropic force chain networks at high pressures.

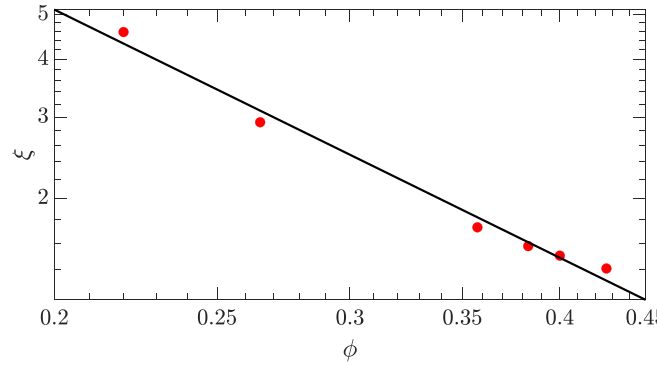

FIG. 7. The correlation length, ξ, is plotted as a function of packing fraction, ϕ. The solid line represents the power-law fit with a slope of -1.78 ± 0.05.

V. LOCAL VOLUME FRACTION FLUCTUATIONS AND HYPERUNIFORMITY

The transition from fluid to solid-like phase across diverse amorphous materials presents many mechanical similarities in terms of finite modulus, yield stress, etc., which can be captured under a common notion of "jamming" [34]. The jamming transition in the amorphous materials happens without any apparent structural signature; i.e., the particle configuration remains disordered in the solid-like phase similar to the liquid phase. But, the exhibition of solid-like properties in the absence of the long-range crystalline order must be due to some long-range pair correlations. Previous studies on the granular materials [35–37] and many other systems [38] indeed presented the existence of a long-ranged direct correlation function which is a direct consequence of the hyperuniformity, i.e., the unusual suppression of density fluctuations in the long-wavelength limit. In the case of a hyperuniform system of point particles, the structure factor $\mathcal{S}(\underline{q})$ tends to zero in the limit $|\underline{q}| \to 0$, which in real space translates into a slower growth (slower than R^d) of the number

variance of particles in a spherical observation window of radius R in the large-R limit. For finite-size and size-disperse particles, the hyperuniformity condition in the real space demands that the local volume fraction fluctuations decay faster than the inverse of the observation window volume [39], and in the Fourier space, instead of the structure factor, the compressibility [40] vanishes in the low-wave-number limit. Although most of the studies focused on characterizing the local density fluctuations in the frictionless granular materials jammed at very high packing fractions and established a link between the hyperuniformity and the jammed state, very few studies were directed toward exploring the long-wavelength density fluctuations in systems jammed at comparatively low packing fractions such as colloidal gel, colloidal glass, and frictional granular materials. To understand the commonalities or lack thereof between diverse jammed systems, characterization of the long length scale density fluctuations is of great fundamental interest. The virial stress tensor in the smaller subvolumes of the system is given by the volume average of the dyadic products between the contact forces and the branch vector over all the contacts in that subregion, $\sigma_{\alpha\beta} = \frac{1}{V}\sum_{j\neq i}\frac{r_{ij}^{\alpha}F_{ij}^{\beta}}{2}$. As per this definition, the spatial stress fluctuations will depend on the number density fluctuations, which translates into the local volume fraction fluctuations for finite-size particles. Hence, we believe that the local density fluctuations will also influence the fluctuations of the local pressure in the jammed amorphous system and ultimately dictate the long-distance decay of the pressure correlations.

Accordingly, to understand the structural origin of the abnormal or normal pressure fluctuations under a common framework, we compute the local volume fraction fluctuations as it provides the appropriate structural descriptions of these disordered packings. We randomly place a circle of radius R within the system and measure the local volume fraction within this window [39,41]. Similarly to the pressure variance, we measure the variance of the packing fraction, $V_\phi(R) \equiv \langle\phi(R)^2\rangle - \langle\phi(R)\rangle^2 \sim \frac{1}{R^{d+\alpha}}$, where exponent α expresses the degree of uniformity [41]. For normal uniformity, $\alpha = 0$; for hyperuniform systems (disordered isotropic systems where long-wavelength fluctuations are suppressed), $\alpha > 0$; and $\alpha < 0$ denotes hyperfluctuations observed in fractal networks [42]. We also simulated frictional and frictionless granular materials per the recent works [11,12] to measure the real-space packing fraction fluctuations. For the granular simulation, we used an amorphous granular assembly of $N = 16\,000$ disks, half of which have a radius 0.35 and the other half with a radius 0.49. Here, for completeness, we show the pressure fluctuations in real space in Fig. 8 for frictional and frictionless materials as per our recent works [11,12]. In Fig. 9, we plot the variance of the local packing fraction V_ϕ as a function of R for colloidal gel ($P = 2.75$ and $P = 328$; here $\mu = 0.5$) and the granular materials ($\mu = 0$ and $\mu = 0.5$; here $P = 72$). The colloidal gel network at low pressure shows hyperfluctuations; i.e., the local packing fraction fluctuations decay slower than the reciprocal of the area of the observation window. The gel network at high pressure shows hyperuniformity as the exponent of the decay of V_ϕ is greater than 2. We also simulated a larger system size ($N = 10^5$) for the colloidal gel system to explore the

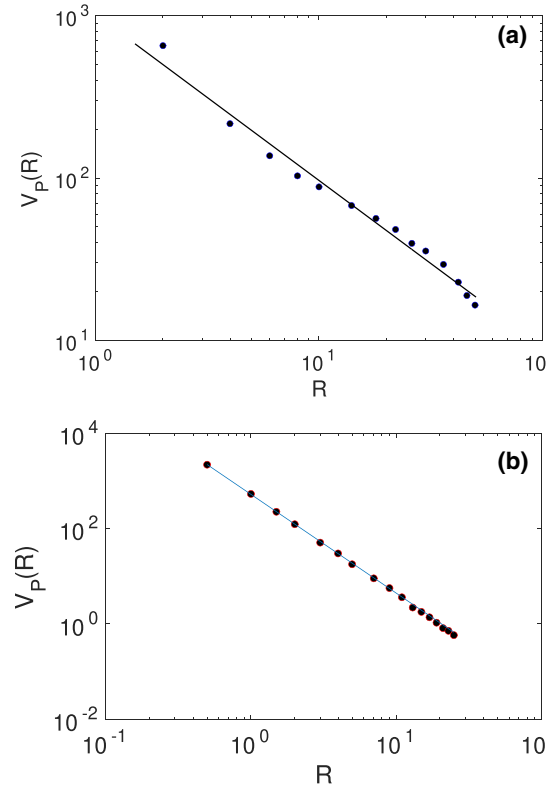

FIG. 8. The variance of pressure, $V_P(R)$, as a function of radius of the probing circular window [11,12]. (a) Frictional granular matter. The solid line is the best linear fit with $V_P(R) \approx \frac{1}{R}$. (b) Frictionless granular matter: The solid line is the best linear fit with $V_P(R) \approx \frac{1}{R^2}$.

packing fraction fluctuation at a larger length scale compared to what could be explored in the smaller system without any finite-size corrections. Figure 10 presents the local packing fraction variance for the large colloidal gel system under low and high pressure. A similar picture emerges to that of the smaller system size: the low-pressure gel shows hyperfluctuations and the high-pressure gel hugely suppresses the packing fraction fluctuations, mimicking a hyperuniform organization of the constituent particles. Similarly, the frictionless granular materials also show hyperuniform behavior with respect to the local packing fraction fluctuations (R^{-3} decay). Lastly, the frictional granular materials do not exhibit hyperuniformity; rather they show *uniform behavior* like $1/R^2$ decay similar to disordered liquids.

To further strengthen our real-space results of the density fluctuations, we additionally compute the structure factor $\mathcal{S}(\underline{q})$ for the monodisperse colloidal gel system [35] and the isothermal compressibility [40], $\chi(\underline{q})$, for the bidisperse granular system. For the monodisperse system, the density fluctuations are hyperuniform provided the structure factor $\mathcal{S}(q)$ tends to zero as the wave number $q \to 0$. For the size-dispersed systems, $\mathcal{S}(q)$ exhibits no unusual suppression in the low-wave-number limit; instead, the isothermal compressibility $\chi(q)$ tends to zero as $q \to 0$. The static structure factor is calculated by taking a direct Fourier transform of the particle positions and angularly averaging over all $\underline{q}$ of equal

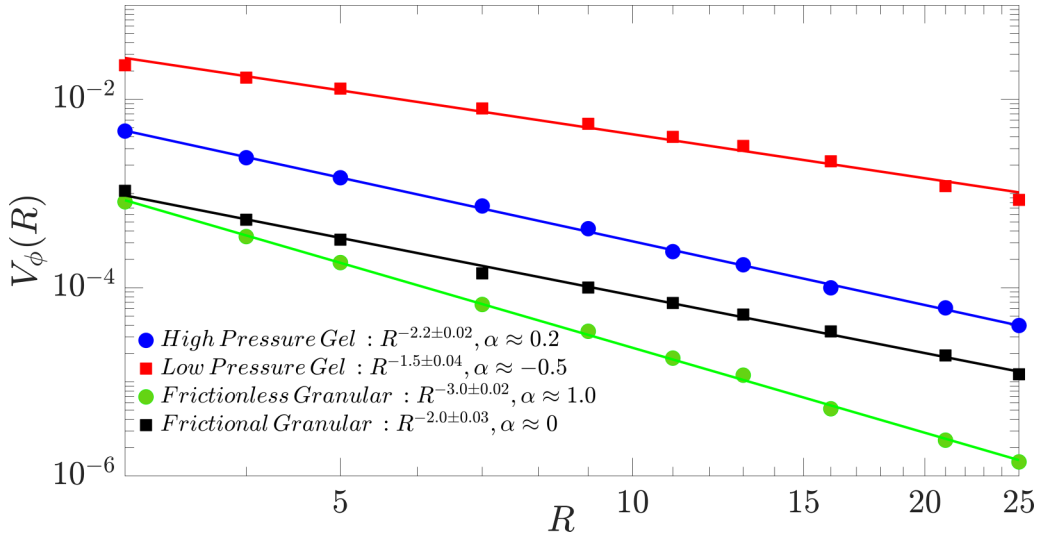

FIG. 9. Variance of the local packing fraction, V_ϕ vs R, as observed in granular materials and gels. The solid line is the best linear fit and represents the power-law scaling.

magnitude q [35,39,43]:

$$\mathcal{S}(q) = \frac{1}{N}\left|\sum_{i=1}^{i=N} \exp(i\underline{q}\cdot\underline{r}_i)\right|^2. \tag{7}$$

For calculating the compressibility $\chi(q)$ for a size-dispersed system, the partial structure factors are first calculated as [40]

$$\mathcal{S}_{ij}(q) = \frac{1}{N}\langle\rho_i(\underline{q})\rho_j(-\underline{q})\rangle, \tag{8}$$

where $\rho_i(\underline{q})$ represents the partial density fields and given as $\rho_i(\underline{q}) = \sum_{j=1}^{N_i}\exp(i\underline{q}\cdot\underline{r}_j)$. N_i denotes the number of particles in species i such that the total number of particles $N = \sum N_i$. Let us also denote the species concentration as c_i, which is given as N_i/N and the density, $\rho = N/V$. For a bidisperse system, the compressibility is given as [40,44]

$$\rho k_B T\chi(q) = \frac{\mathcal{S}_{11}(q)\mathcal{S}_{22}(q) - \mathcal{S}_{12}^2(q)}{c_1^2\mathcal{S}_{22}(q) + c_2^2\mathcal{S}_{11}(q) - 2c_1c_2\mathcal{S}_{12}(q)}, \tag{9}$$

where k_B is Boltzmann's constant and T is temperature.

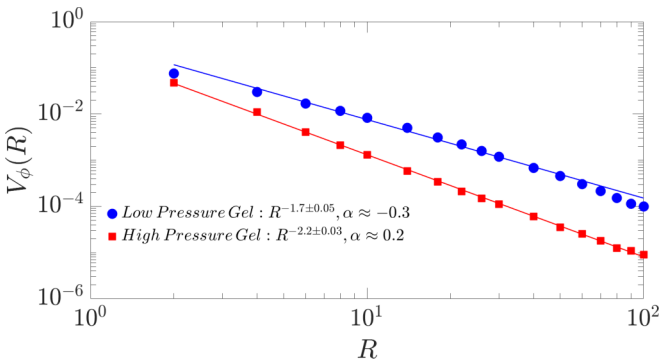

FIG. 10. Variance of the local packing fraction, V_ϕ vs R, as observed in colloidal gels for large system size, $N = 100\,000$. The solid line is the best linear fit and represents the power-law scaling.

In Fig. 11, we present a comparative picture of the structure factor and compressibility data for diverse jammed amorphous materials. For monodisperse colloidal gel systems at low pressure, the structure factor $\mathcal{S}(q)$ diverges in the limit of small wave number, representing hyperfluctuations, which is the antithesis of a hyperuniform system. Unboundedness of $\mathcal{S}(q)$ in the low-q limit gives rise to slower than normal decay of the packing fraction fluctuations on domains of increasing size. On the contrary, the gel system when compressed to a high pressure shows almost a linear decay of the structure factor as the small-wave-number limit is approached. Hence, the gel system suppresses the density fluctuations in the limit of large length scale upon compression to higher pressure. Also, for the bidisperse frictionless granular system, compressibility displays anomalous low-q linear decay

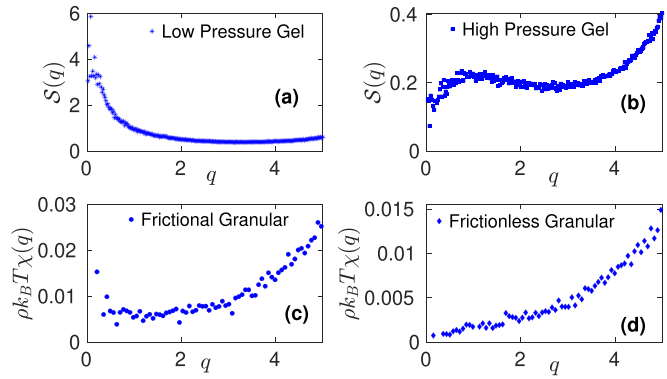

FIG. 11. (a) Structure factor for the low-pressure colloidal gel ($P = 2.75$ and $\phi = 0.22$) for the largest system investigated ($N = 10^5$). (b) Structure factor for the colloidal gel system at high pressure ($P = 328$ and $\phi = 0.44$) for the largest system investigated ($N = 10^5$). (c) Compressibility for the bidisperse frictional granular materials above the jamming point ($P = 72$ and $\phi = 0.81$). Here, $N = 16\,000$. (d) Compressibility data for the bidisperse frictionless granular materials above the jamming point ($P = 72$ and $\phi = 0.84$). Here, $N = 16\,000$.

representative of hyperuniform density fluctuations. Conversely, in the presence of friction, the compressibility for granular systems plateaus to a finite positive value for $q \to 0$ and shows no sign of decay. Hence, the frictional granular matter certainly does not belong to a hyperuniform system. This is the most interesting result of this work as it establishes a strong link between the abnormal pressure fluctuations and the non-hyperuniform behavior of the many-particle systems. The normal elastic decay of stress correlations is intimately linked to the long-wavelength suppression of the local packing fraction fluctuations, i.e., hyperuniform behavior. This observation points to some sort of nontrivial self-organization of the disordered network in exhibiting the normal elastic behavior. The self-organization is controlled by the mechanical and topological constraints. For frictionless materials, although the structural arrest takes place at high packing fractions, the particles can rearrange easily through sliding whereas in frictional material, the sliding is constrained by the Coulomb friction which frustrates the relaxation of the density inhomogeneities. The positivity constraint on the normal force is released in the colloidal gel system and as the structural arrest takes place at low packing fraction, the system can reorganize and minimize the density fluctuations at high pressure.

VI. SUMMARY

In conclusion, we convincingly demonstrate that under the mechanical balance and material isotropy constraints, the full stress autocorrelation matrix in soft gel materials is determined by the torque and pressure autocorrelations similarly to frictional granular matter, thus suggesting a universal behavior across diverse amorphous solids. Interestingly, close to the gel point, we observe the divergence in pressure correlations in the $q \to 0$ limit and non-hyperuniform torque correlations whose contribution to the stress correlations at long length scale is subdominant and the pressure fluctuation statistics strongly determine the exponent of the divergence. We have also linked this divergence to inhomogeneous and anisotropic force networks formed due to the presence of large voids at low packing fractions. At high pressure, the system shows almost divergence-free elastic behavior with hyperuniform torque fluctuations and the normal pressure decay as the large voids collapse and the system has enough space to relax the force inhomogeneities which is not possible for the frictional granular matter jammed at high packing fractions. Most importantly, we identify a connection between the abnormal pressure fluctuations and the non-hyperuniform behavior of the system with respect to the local packing fraction fluctuations, thus establishing a common framework to understand the deviations from the normal elastic like behavior across different jammed systems. The result of this work begs for the development of a novel theoretical framework to understand the mechanical response of gel at low pressure and real granular materials as these systems clearly deviate from the normal elastic behavior as shown. This work provides a plausible understanding of the physical mechanism behind ultra-long-ranged cooperative dynamics with the help of long-range stress correlations. Although we expect our results to be generic and unaffected by the spatial dimension, future work will focus on confirming the same in three dimension.

ACKNOWLEDGMENTS

S.R. acknowledges the support of SERB under Grant No. SRG/2020/001943. C.M. acknowledges funding from SERB (Ramanujan Fellowship, File No. RJF/2021/00012).

[1] Y. M. Joshi, Annu. Rev. Chem. Biomol. Eng. **5**, 181 (2014).
[2] A. Duri, D. A. Sessoms, V. Trappe, and L. Cipelletti, Phys. Rev. Lett. **102**, 085702 (2009).
[3] Y. Wu, K. Karimi, C. E. Maloney, and S. Teitel, Phys. Rev. E **96**, 032902 (2017).
[4] S. Henkes and B. Chakraborty, Phys. Rev. E **79**, 061301 (2009).
[5] A. Lemaître, Phys. Rev. Lett. **113**, 245702 (2014).
[6] B. Wu, T. Iwashita, and T. Egami, Phys. Rev. E **91**, 032301 (2015).
[7] A. Lemaître, J. Chem. Phys. **143**, 164515 (2015).
[8] S. Maccarrone, G. Brambilla, O. Pravaz, A. Duri, M. Ciccotti, J.-M. Fromental, E. Pashkovski, A. Lips, D. Sessoms, V. Trappe *et al.*, Soft Matter **6**, 5514 (2010).
[9] J. Colombo and E. Del Gado, Soft Matter **10**, 4003 (2014).
[10] M. Bouzid, J. Colombo, L. V. Barbosa, and E. Del Gado, Nat. Commun. **8**, 15846 (2017).
[11] A. Lemaître, C. Mondal, I. Procaccia, S. Roy, Y. Wang, and J. Zhang, Phys. Rev. Lett. **126**, 075501 (2021).
[12] A. Lemaître, C. Mondal, I. Procaccia, and S. Roy, Phys. Rev. B **103**, 054110 (2021).
[13] A. Lemaître, Phys. Rev. E **96**, 052101 (2017).
[14] F. Bonacci, X. Chateau, E. M. Furst, J. Fusier, J. Goyon, and A. Lemaître, Nat. Mater. **19**, 775 (2020).
[15] F. Bonacci, X. Chateau, E. M. Furst, J. Goyon, and A. Lemaître, Phys. Rev. Lett. **128**, 018003 (2022).
[16] S. Plimpton, J. Comput. Phys. **117**, 1 (1995).
[17] N. Y. C. Lin, B. M. Guy, M. Hermes, C. Ness, J. Sun, W. C. K. Poon, and I. Cohen, Phys. Rev. Lett. **115**, 228304 (2015).
[18] G. Brambilla, S. Buzzaccaro, R. Piazza, L. Berthier, and L. Cipelletti, Phys. Rev. Lett. **106**, 118302 (2011).
[19] Z. Varga, G. Wang, and J. Swan, Soft Matter **11**, 9009 (2015).
[20] J. Colombo and E. Del Gado, J. Rheol. **58**, 1089 (2014).
[21] J. P. Pantina and E. M. Furst, Phys. Rev. Lett. **94**, 138301 (2005).
[22] E. M. Furst and J. P. Pantina, Phys. Rev. E **75**, 050402(R) (2007).
[23] B. van der Meer, T. Yanagishima, and R. P. A. Dullens, arXiv:2209.12703.
[24] A. Boromand, S. Jamali, B. Grove, and J. M. Maia, J. Rheol. **62**, 905 (2018).
[25] S. Roy and M. S. Tirumkudulu, Soft Matter **12**, 9402 (2016).
[26] S. Roy and M. S. Tirumkudulu, J. Rheol. **60**, 559 (2016).
[27] S. Roy and M. S. Tirumkudulu, J. Rheol. **60**, 575 (2016).
[28] M. Islam and D. Lester, J. Rheol. **65**, 837 (2021).
[29] Y. A. Gadi Man, D. S. Dagur, and S. Roy, J. Chem. Phys. **158**, 124902 (2023).

[30] P. A. Cundall and O. D. Strack, Géotechnique **29**, 47 (1979).
[31] S. Luding, Granular Matter **10**, 235 (2008).
[32] F. A. Gilabert, J.-N. Roux, and A. Castellanos, Phys. Rev. E **78**, 031305 (2008).
[33] D. J. Evans and G. Morriss, *Statistical Mechanics of Nonequilibrium Liquids* (Cambridge University Press, 2008).
[34] A. J. Liu and S. R. Nagel, Nature (London) **396**, 21 (1998).
[35] L. E. Silbert and M. Silbert, Phys. Rev. E **80**, 041304 (2009).
[36] A. Donev, F. H. Stillinger, and S. Torquato, Phys. Rev. Lett. **95**, 090604 (2005).
[37] C. E. Zachary, Y. Jiao, and S. Torquato, Phys. Rev. Lett. **106**, 178001 (2011).
[38] J. H. Weijs, R. Jeanneret, R. Dreyfus, and D. Bartolo, Phys. Rev. Lett. **115**, 108301 (2015).
[39] C. E. Zachary, Y. Jiao, and S. Torquato, Phys. Rev. E **83**, 051308 (2011).
[40] L. Berthier, P. Chaudhuri, C. Coulais, O. Dauchot, and P. Sollich, Phys. Rev. Lett. **106**, 120601 (2011).
[41] S. Torquato, Phys. Rep. **745**, 1 (2018).
[42] A. Wax, C. Yang, V. Backman, K. Badizadegan, C. W. Boone, R. R. Dasari, and M. S. Feld, Biophys. J. **82**, 2256 (2002).
[43] N. Xu and E. S. Ching, Soft Matter **6**, 2944 (2010).
[44] A. Bhatia and D. Thornton, Phys. Rev. B **2**, 3004 (1970).